


X-Ray Tomography Investigation of Cyclically Sheared Granular Materials

Yi Xing,¹ Jie Zheng,¹ Jindong Li,¹ Yixin Cao,¹ Wei Pan,¹ Jie Zhang,^{1,2} and Yujie Wang^{1,3,*}

¹*School of Physics and Astronomy, Shanghai Jiao Tong University, 800 Dong Chuan Road, Shanghai 200240, China*

²*Institute of Natural Sciences, Shanghai Jiao Tong University, Shanghai 200240, China*

³*Materials Genome Initiative Center, Shanghai Jiao Tong University, 800 Dong Chuan Road, Shanghai 200240, China*

 (Received 4 July 2020; revised 24 October 2020; accepted 4 January 2021; published 27 January 2021)

We perform combined x-ray tomography and shear force measurements on a cyclically sheared granular system with highly transient behaviors, and obtain the evolution of microscopic structures and macroscopic shear force during the shear cycle. We explain the macroscopic behaviors of the system based on microscopic processes, including particle level structural rearrangement and frictional contact variation. Specifically, we show how contact friction can induce large structural fluctuations and cause significant shear dilatancy effect for granular materials, and we also construct an empirical constitutive relationship for the macroscopic shear force.

DOI: [10.1103/PhysRevLett.126.048002](https://doi.org/10.1103/PhysRevLett.126.048002)

Dense granular materials exhibit complex behaviors upon shear. Notable examples include significant dilatancy [1], formation of shear bands [2], emergence of anisotropic force networks [3], and critical state [4]. However, the theoretical understanding of sheared granular materials remains very challenging since conventional continuum mechanics are no longer applicable due to the disordered nature of granular materials, as well as the complex role friction plays [5,6]. In practice, empirical constitutive theories are normally employed, including the famous Mohr-Coulomb criterion [7] and more sophisticated viscoplastic models [8]. However, these models are mainly macroscopic ones with little microscopic basis despite the fact that it is well known experimentally that microscopic structure and dynamics can strongly influence the macroscopic response [9]. Granular materials belong in general to the family of disordered materials like metallic and colloidal glasses, foams, emulsions, etc., and physicists have tried to treat the flow of dense granular materials within the general framework of disordered materials [9]. For example, theories based on free volume [10], shear transformation zone [11], and soft glass rheology (SGR) theories [12], which are built upon microscopic and mesoscopic information to predict the plastic behaviors of certain disordered materials, have been directly applied to the granular case [13,14]. However, granular materials possess some peculiar properties, e.g., force chains [15,16], significant volume and stress fluctuations [6,17,18], and complex microscopic dynamics [19], which are not shared among all disordered materials. These properties are mainly induced by the frictional interparticle contacts. Therefore, to construct the correct constitutive theory for the flow of dense granular materials, physics on particle and contact levels have to be considered [20].

In this Letter, we apply cyclic shear to a three-dimensional (3D) disordered granular system. The system displays

highly transient dilatational behavior and mechanical response since the system always has to reorganize upon sudden shear reversal [14,21]. By combing x-ray tomography and shear force measurements, we obtain both microscopic structure evolution and macroscopic mechanical response of the system simultaneously. Based on these results, we can explain the macroscopic behaviors of sheared granular matter through the microscopic structural information including both particle level structural rearrangement and frictional contact evolution. We can then understand why granular materials demonstrate significant shear dilation as compared to other disordered materials, and also construct an empirical constitutive relationship to account for the macroscopic shear force behavior.

Our granular system consists of bidisperse smooth plastic beads ($\mu = 0.4$, diameters 5 and 6 mm, 7000 particles of each size). The bidisperse nature ensures no crystallization occurs in the system. The particles are placed in a shear cell mounted on a linear stage as shown in Fig. 1(a). The shear cell is in simple shear geometry and has an inner dimension of $24d \times 24d \times 24d$, where

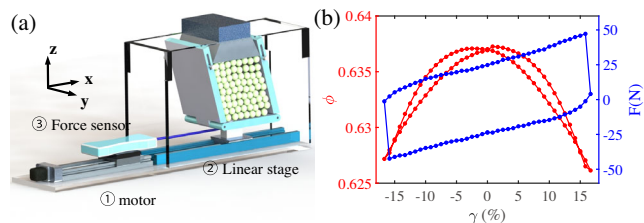


FIG. 1. (a) Schematic of the experimental setup: granular packing is sheared by the motor on the linear stage, and the macroscopic shear force is measured by the force sensor. (b) Evolutions of the global volume fraction ϕ and shear force F within one cycle (ensemble averaged over 12 realizations).

$d = 5$ mm is the small particle's diameter and is set as the unit length. A lid that can freely translate vertically is placed on top of the particle packing (3.6 kg, about 3 times of the total particle weight) to maintain a constant pressure and reduce the vertical pressure gradient. Shear is generated by a stepping motor attached to the bottom plate of the shear cell through a linear stage. A force sensor (IMADA ZTS-50N) connecting the motor and the stage is used to measure the shear force.

We prepare the initial state of the system by applying thousands of cyclic shear cycles which ensures that a steady state is reached [19]. The shear strain amplitude we apply is $\gamma = 0.167$ and the strain rate is $\dot{\gamma} = 0.25$ s⁻¹. The corresponding inertial number is $I = \dot{\gamma}d/\sqrt{P/\rho} = 3 \times 10^{-4}$, suggesting that the system is in a quasistatic regime. After the initial preparation, we divide one shear cycle into 80 steps and an x-ray tomography scan is performed after each shear step through a medical CT scanner (UEG Medical Group Ltd., 0.2 mm spatial resolution). Following similar image processing procedures as previous studies [22], the sizes and positions of all particles are obtained with an uncertainty less than $3 \times 10^{-3}d$ through a marker-based watershed segmentation technique. Using the particle tracking algorithm [23], we can then extract the trajectories and contact geometries of all particles. Simultaneously, the shear force is measured at a frequency of 0.23 s⁻¹ and with an accuracy of 0.1N. For better statistics, the measurements are repeated for consecutive 12 shear cycles. More details about the experimental setup and the image processing procedures can be found in [23].

We calculate the global volume fraction ϕ based on radical Voronoi tessellation [24]: $\phi = \sum V_g / \sum V_{\text{voroi}}$, where V_g and V_{voroi} are each particle's volume and corresponding Voronoi cell volume. To exclude the boundary effect, the structural analysis only involves particles that are at least $2d$ away from the boundary of the shear cell. Figure 1(b) shows the evolution of ϕ and shear force F of the system within one cycle. Starting from the initial symmetric state (shear strain $\gamma = 0$), ϕ decreases as the strain γ increases, then ϕ returns to almost the same initial value as the shear is totally reversed with small hysteresis. The similar behavior is repeated for the other half shear cycle. While for the shear force F , starting from the symmetric state, it increases as the strain γ increases; at the shear reversal point, F changes its direction and its magnitude drops abruptly to almost zero, then it increases monotonically till the next shear reversal point.

Empirical constitutive relations are ordinarily employed to account for macroscopic behaviors, e.g., ϕ and F , of sheared granular materials [8]. However, it is important to develop theories which construct these relations based on microscopic information [25]. Following this approach, we characterize the microscopic structure of our system by Delaunay tessellation and extract the microscopic origin of

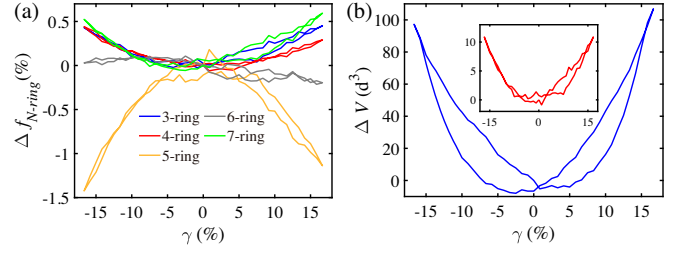


FIG. 2. (a) Variation of fractions of N -ring structures $\Delta f_{N\text{-ring}}$ within one cycle with respect to the symmetric states ($\gamma = 0$), where $\Delta f_{N\text{-ring}} = f_{N\text{-ring}}(\gamma) - f_{N\text{-ring}}(\gamma = 0)$. (b) Volume change ΔV_{global} and ΔV_{topo} (inset) within one cycle.

macroscopic behaviors by analyzing the structural and topological evolutions of the Delaunay network upon shear.

Delaunay tessellation partitions the packing structure into nonoverlapping tetrahedra, whose vertices are the centers of four neighboring particles. Upon shear, as the structure of the system varies, the corresponding Delaunay tetrahedra distort gradually and are destroyed when local neighbor switching process occurs, which changes the local topology of the network [22]. We use N -ring structure, i.e., a tetrahedral group consisting of N tetrahedra sharing one common edge, instead of tetrahedron to characterize the topological change and distortion of the Delaunay network. This is owing to the fact that physically N -ring structures are presumed to be closely related to glass transition in disordered materials, where 5-ring structures are considered as the glass order and other N -ring structures as disclination defects in spherical particle systems without too much polydispersity [26]. Each topological change, or flip process [22], corresponds to the creation or destruction of N -ring defects while its relationship with tetrahedron is less straightforward. N -ring analysis can therefore help establish a physically intuitive understanding of topological change or rearrangement-induced global volume variation based on the creation or destruction of N -ring defects. Moreover, since each N -ring structure is simply an assembly of tetrahedra, so analysis of the distortion process of Delaunay network remains the same based on either N -ring structure or tetrahedron.

We first show how topological rearrangement and distortion of N -ring structures can lead to the global volume variation of our system. As shown in Fig. 2(a), upon shear, the fraction of different N -ring structures $f_{N\text{-ring}}$ (the number ratio between a specific type of N -ring structures and all types) evolves with γ . Within one cycle, the overall trend is that the fraction of 5-ring structures decreases as the system moves away from the symmetric state and the fractions of 3-, 4-, and 7-ring structures increase correspondingly, while the fraction of 6-ring structures remains nearly constant during the cycle. Nevertheless, variations are less than 2% from the symmetric state. For disordered materials, excess volumes are ordinarily related to defective

structures [13]. This is consistent with the observation that an increase of the total volume of the system ΔV_{global} [Fig. 2 (b)] is correlated with the increase of defective (3-, 4-, 6-, 7-) N -ring structures [Fig. 2(a)] and the decrease of 5-ring structures. To quantify the volume change associated with topological rearrangement, the excess volume of each type of N -ring defective structures needs to be obtained. We show subsequently that the appearance of defective structures can be viewed as the excitation process governed by certain effective temperature, similar to the framework of shear transformation zone theory of disordered materials [11].

Since our system has reached steady state by initial preparation, we adopt the granular thermodynamic framework originally developed by Edwards and co-workers [27]. Within this framework, volume plays the role similar to energy in ordinary thermal system and an effective granular temperature, i.e., compactivity χ , can be obtained based on its fluctuation. We find the use of an effective granular temperature can greatly help us understand our experimental observations.

Following the method proposed by Aste [28], we obtain compactivity χ based on the free volume v_f distribution of Delaunay tetrahedron, where $v_f = v_T - v_g$, v_T is the volume of each Delaunay tetrahedron, and v_g is the corresponding volume of particles within the Delaunay tetrahedron. If the system is in thermal equilibrium based on Edwards statistical framework and under the constraint of constant total volume, the probability of finding a tetrahedron possessing a specific free volume v_f should follow an exponential distribution, as can be derived from standard statistical mechanics [28]. As shown in Fig. 3(a), indeed the exponential behavior is found in the probability distribution function (PDF) of the tetrahedron in the large free volume region. This exponential behavior remains robust within the whole shear cycle albeit its slope varies. The slope change corresponds to the variation of the compactivity χ and its evolution within one cycle is shown in the inset of Fig. 3(a). Nevertheless, the PDFs are not exponential in the small volume regime which remains unchanged upon shear. This is due to the fact that the distributions of these small volume tetrahedra are mainly governed by the mechanical stability of the local Delaunay network topology and are less related to χ [28].

Analogous to the thermal excitation of point defects in crystals, we presume that the numbers of different N -ring structures are governed by χ and follow Boltzmann distribution depending on their respective excitation volumes [29], i.e., $N_{N\text{-ring}}/N_{5\text{-ring}}$ and $-1/\chi$ satisfy

$$\frac{N_{N\text{-ring}}}{N_{5\text{-ring}}} \sim \exp\left(-\frac{E_{N\text{-ring}}}{\chi}\right), \quad (1)$$

where $N_{N\text{-ring}}$ is the number of respective N -ring structure and $E_{N\text{-ring}}$ is its corresponding mean excitation volume

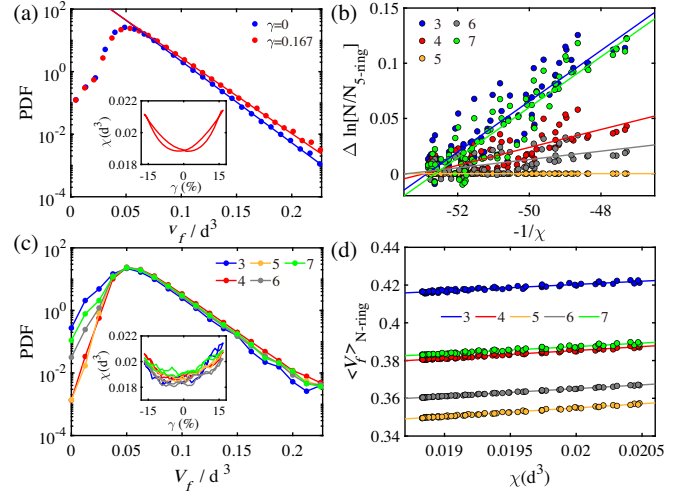


FIG. 3. (a) Probability distribution functions of the Delaunay tetrahedron free volume v_f at $\gamma = 0$ and $\gamma = 0.167$. The solid lines denote the exponential fittings on tails. Inset: evolution of the effective temperature χ within one cycle. (b) Relationship between $\Delta \ln(N_{N\text{-ring}}/N_{5\text{-ring}})$ and $-1/\chi$. All lines are shifted vertically to have zero intercepts on the vertical axis. (c) Probability distribution functions of Delaunay tetrahedron free volume v_f of different N -ring structures at $\gamma = 0.167$. Inset: evolution of effective temperatures for different N -ring structures within one cycle which are obtained from exponential fittings of their respective tails in the main plot. (d) Relationship between $\langle V_f \rangle_{N\text{-ring}}$ and χ for different types of N -ring structures.

from the 5-ring ground state in our system. In Fig. 3(b), we plot $N_{N\text{-ring}}/N_{5\text{-ring}}$ as functions of $-1/\chi$ on a semi-logarithmic plot. All relationships are clearly linear which is compatible with the existence of the Boltzmann distribution and the thermal excitation scenario. We extract the excitation volume $E_{N\text{-ring}}$ of each type of N -ring structure by fitting the slopes of the curves and obtain the corresponding excitation volume for 3-, 4-, 5-, 6-, and 7-ring structures as 0.023, 0.008, 0, 0.004, and 0.023 d^3 , respectively. After we obtain $E_{N\text{-ring}}$, we then calculate the total excitation volume resulting from the population change of different N -ring structures: $\Delta V_{\text{topo}} = \sum E_{N\text{-ring}} \times \Delta N_{N\text{-ring}}$, where $\Delta N_{N\text{-ring}}$ is the number change of each type of N -ring structure from the symmetric state. The result is shown in Fig. 2(b) and counterintuitively, we find that only 10% of the total volume change ΔV_{global} originates from ΔV_{topo} .

The rest volume change instead results from the mean free volume change of N -ring structures induced by Delaunay network distortion. We calculate the normalized mean N -ring structure free volume $\langle V_f \rangle_{N\text{-ring}}$ by dividing the mean free volume of each type of N -ring structure with its respective mean total volume. As shown in Fig. 3(d), we find that $\langle V_f \rangle_{N\text{-ring}}$ depends linearly on χ for all N -ring structures. Other than the intercept differences between different lines, the slopes are almost the same. If we simply fix the number of different N -ring structures during shear

and only monitor the total volume change using above linear relationship with χ , we find it makes up the 90% volume change not accounted for by topological rearrangements. We note that this behavior is not accidental and originates from the behaviors of constituting tetrahedra. As shown in Fig. 3(c), we plot the PDFs of volume v_f of tetrahedra which make up each type of N -ring structure. We find that in the small v_f region, the PDFs of all N -ring structures do not change with χ ; in the large v_f region, the PDFs of all N -ring structures exhibit same slope exponential tails governed by χ [inset of Fig. 3(c)]. As χ increases upon shear, the fractions of tetrahedra possessing large v_f increase which leads to the increase of mean free volume of N -ring structures.

Physically, the variation of mean free volume of N -ring structures originates from a contact-friction-induced fluctuation effect: upon shear, due to the presence of contact friction, topological rearrangement among different N -ring structures does not happen instantaneously [19,22]. Instead, N -ring structures will gradually distort before a topological rearrangement occurs. These friction-stabilized highly distorted structures can induce large volume fluctuations, as is clear from above observation that the average volume change among different N -ring structures (topological rearrangements) is actually quite small as compared to the friction-induced distortion effect. To quantify the magnitude of this fluctuation effect, we find that the dimensionless effective temperature of our system is around 0.02 which is significantly larger than the values of other sheared disordered systems [30,31] (normally on the order of 10^{-3}). Specifically, the dimensionless effective temperature is obtained by normalizing the energy scale of the effective temperature $p\chi = 0.02pd^3$, by the energy required to move one particle by its own diameter which is about pd^3 , where p is the pressure. The one order of magnitude difference suggests that friction can significantly enhance fluctuations in granular systems and can explain why granular materials exhibit much larger shear dilatancy effect than frictionless hard sphere system [32] and other disordered materials [30,31], since topological rearrangement is the only mechanism for dilation for those materials.

Other than volume, we also seek the microscopic structural origin of macroscopic shear force response through the evolution of the Delaunay network. For disordered systems, macroscopic shear stress is normally related to the plastic processes induced by topological rearrangements [33]. However, in sheared granular materials, energy dissipation happens both as the local structure undergoes a topological rearrangement and frictional contact evolution [34], the macroscopic mechanical response can be reasonably understood only after considering both processes. In the following, we show that an empirical constitutive relationship can well explain the global shear force variation using microscopic structural information

including both topological rearrangement of the Delaunay network and contact fabric evolution induced by Delaunay network distortion.

Local topological rearrangements not only induce volume fluctuations, but they also relax stress in the system and therefore should be strongly correlated with macroscopic shear force. This correlation has been identified previously as we found that topological rearrangements or flip events mainly occur along principal stress directions [22]. Before establishing the relationship between topological rearrangement and shear force F , we note that both of them have orientations and a full analysis will need a tensorial description. To develop a full thermodynamic theory for the shear force, a tensorial effective temperature, e.g., anisotropy, based on microscopic stress fluctuations [27], has to be defined, which is clearly beyond the capability of our x-ray technique. Instead, we simplify this tensorial treatment into a scalar one by using a two-state approximation analogous to previous studies [33]. Specifically, we classify all topological rearrangements into two orientation groups according to whether the angle between their orientations and one principal stress direction is smaller than with the other one. We then assume that there exists a simple proportional relation between the number of topological rearrangements with principal stress. Since shear stress is the difference between two principal stresses, we also calculate the net topological rearrangement number curve N_{topo} by calculating the number difference of the two topological rearrangement orientation groups, as shown in Fig. 4(a) (see Supplemental Material [23] for more details). Comparing the N_{topo} curve with the

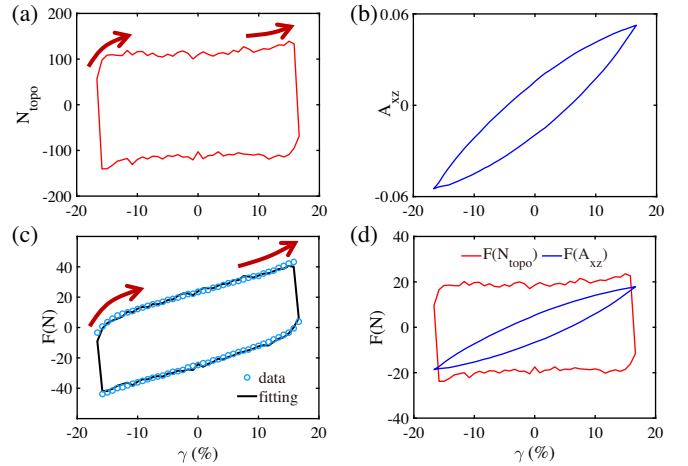


FIG. 4. (a) Evolution of N_{topo} within one cycle. The arrows are guides to eye to show the increasing trends of N_{topo} just before and after shear reversal which is analogous to the behavior of shear force F in (c). (b) Evolution of the A_{xz} component of the fabric tensor within one cycle. (c) Shear force behavior within one cycle and the corresponding empirical fitting using N_{topo} and A_{xz} . (d) The respective contributions of N_{topo} and A_{xz} to shear force F , denoted by $F(N_{\text{topo}})$ and $F(A_{xz})$.

shear force F evolution [Figs. 4(a) and (c)], we find that the significant hysteretic behavior of N_{topo} , the rapid increase of N_{topo} just before shear reversal, and the abrupt drop of it after shear reversal, as shown in Fig. 4(a), are analogous to the behavior of shear force F in Fig. 4(c). However, N_{topo} does not match the upward sloping trend of F .

To account for this disparity, we also have to take Delaunay network distortion-induced contact level variation into account. It is reasonable to presume that the stress variation is linearly related to the variation of contact network as normally characterized by fabric tensor [21,35,36]:

$$\mathbf{A} = \frac{1}{N_c} \sum_{\alpha=1}^{N_c} \mathbf{n}^\alpha \otimes \mathbf{n}^\alpha - \frac{1}{3} \mathbf{I}, \quad (2)$$

where N_c is the total number of contacts, \mathbf{n} is the unit contact normal vector from center to center of two particles in contact, and \mathbf{I} is the unit tensor. This analysis only applies for particles with at least two contacts. We notice that the contact evolution of the system is mainly in A_{xz} component. Therefore, we only use this component to approximate the contact evolution of the system, and its upward sloping trend is consistent with the behavior of F , as shown in Fig. 4(b).

To account for the complex shear force behavior within one cycle, we assume that both particle level topological rearrangement and contact evolution contribute linearly to the shear force F to the first approximation. We adopt an empirical fitting procedure to understand their individual contributions. We normalize the N_{topo} and A_{xz} curves by setting the variation ranges of them to be unity and do the following fitting:

$$F = a \times N_{\text{topo}} + b \times A_{xz}. \quad (3)$$

The fitting result is shown in Fig. 4(c) with the corresponding fitting coefficients $a=47.4N$ and $b=36.7N$, and their respective contributions are shown in Fig. 4(d). From the fitting, it is clear that the shear force behavior can be well accounted for after taking into account both topological rearrangement and contact evolution information. Specifically, N_{topo} can explain the significant hysteresis of F and its rapid variation around the reversal points, while A_{xz} plays a more important role in matching the upward sloping trend of F .

In summary, by taking the friction-induced effect into consideration, combined with the knowledge of particle level topological rearrangements, we can explain the highly transient global volume and the shear force variations of a cyclically sheared granular system. This experimental finding reconciles previous theoretical approaches focusing only on particle or contact scales physics and therefore is a significant step forward to the understanding the flow of dense granular materials [37]. It is worth noting that in our system, the majority 90% volume variation is caused by the

contact-friction-induced Delaunay network distortion and the remaining 10% is induced by topological rearrangements. The importance of the contact friction effect is also reflected in the contribution of contact fabric tensor to the empirical constitutive relationship. However, it is obvious that the specific fraction of contributions from these two microscopic mechanisms should be strongly correlated with the microscopic friction coefficient of granular particles which will be system dependent. It will be interesting to investigate the relative importance of these two mechanisms by varying the friction coefficients of particles in future studies.

The work is supported by the National Natural Science Foundation of China (No. 11974240, No. 11675110, No. U1738120), Shanghai Science and Technology Committee (No. 19XD1402100).

*Corresponding author.
yujiewang@sjtu.edu.cn

- [1] J. Duran, *Sands, Powders, and Grains: An Introduction to the Physics of Granular Materials* (Springer, New York, 2000).
- [2] A. Le Bouil, A. Amon, S. McNamara, and J. Crassous, *Phys. Rev. Lett.* **112**, 246001 (2014).
- [3] T. S. Majmudar and R. P. Behringer, *Nature (London)* **435**, 1079 (2005).
- [4] A. Schofield and P. Wroth, *Critical State Soil Mechanics* (McGraw-Hill, New York, 1968).
- [5] H. M. Jaeger, S. R. Nagel, and R. P. Behringer, *Rev. Mod. Phys.* **68**, 1259 (1996).
- [6] R. R. Hartley and R. R. Behringer, *Nature (London)* **421**, 928 (2003).
- [7] R. M. Nedderman, *Statics and Kinematics of Granular Materials* (Cambridge University Press, Cambridge, England, 1992).
- [8] B. Andreotti, Y. Forterre, and O. Pouliquen, *Granular Media: Between Fluid and Solid* (Cambridge University Press, Cambridge, England, 2013).
- [9] A. Nicolas, E. E. Ferrero, K. Martens, and J.-L. Barrat, *Rev. Mod. Phys.* **90**, 045006 (2018).
- [10] F. Spaepen, *Scr. Mater.* **54**, 363 (2006).
- [11] M. L. Falk and J. S. Langer, *Annu. Rev. Condens. Matter Phys.* **2**, 353 (2011).
- [12] P. Sollich, F. Lequeux, P. Hébraud, and M. E. Cates, *Phys. Rev. Lett.* **78**, 2020 (1997).
- [13] A. Lemaître, *Phys. Rev. Lett.* **89**, 195503 (2002).
- [14] M. L. Falk, M. Toiya, and W. Losert, arXiv:0802.1752 (2008).
- [15] A. Tordesillas, *Philos. Mag.* **87**, 4987 (2007).
- [16] D. Howell, R. P. Behringer, and C. Veje, *Phys. Rev. Lett.* **82**, 5241 (1999).
- [17] D. Denisov, K. Lörincz, J. Uhl, K. A. Dahmen, and P. Schall, *Nat. Commun.* **7**, 10641 (2016).
- [18] C. Song, P. Wang, and H. A. Makse, *Proc. Natl. Acad. Sci. U.S.A.* **102**, 2299 (2005).
- [19] B. Kou, Y. Cao, J. Li, C. Xia, Z. Li, H. Dong, A. Zhang, J. Zhang, W. Kob, and Y. Wang, *Nature (London)* **551**, 360 (2017).

- [20] T. Stegmann, J. Török, L. Brendel, and D. E. Wolf, *Granular Matter* **13**, 565 (2011).
- [21] J. Sun and S. Sundaresan, *J. Fluid Mech.* **682**, 590 (2011).
- [22] Y. Cao *et al.*, *Nat. Commun.* **9**, 2911 (2018).
- [23] See Supplemental Material at <http://link.aps.org/supplemental/10.1103/PhysRevLett.126.048002> for details regarding the experimental setup, image processing procedures, and the calculation of net topological rearrangement number curve.
- [24] C. Rycroft, *Chaos* **19**, 041111 (2009).
- [25] N. Kumar, S. Luding, and V. Magnanimo, *Acta Mech.* **225**, 2319 (2014).
- [26] D. R. Nelson and F. Spaepen, *Solid State Phys.* **42**, 1 (1989).
- [27] D. Bi, S. Henkes, K. E. Daniels, and B. Chakraborty, *Annu. Rev. Condens. Matter Phys.* **6**, 63 (2015).
- [28] T. Aste, *Phys. Rev. Lett.* **96**, 018002 (2006).
- [29] A. Argon, *Acta Metall.* **27**, 47 (1979).
- [30] I. K. Ono, C. S. O'Hern, D. J. Durian, S. A. Langer, A. J. Liu, and S. R. Nagel, *Phys. Rev. Lett.* **89**, 095703 (2002).
- [31] E. I. Corwin, H. M. Jaeger, and S. R. Nagel, *Nature (London)* **435**, 1075 (2005).
- [32] P. E. Peyneau and J. N. Roux, *Phys. Rev. E* **78**, 011307 (2008).
- [33] M. L. Falk and J. S. Langer, *Phys. Rev. E* **57**, 7192 (1998).
- [34] N. P. Kruyt and L. Rothenburg, *J. Mech. Phys. Solids* **95**, 411 (2016).
- [35] D. Bi, J. Zhang, B. Chakraborty, and R. P. Behringer, *Nature (London)* **480**, 355 (2011).
- [36] M. Schwartz and R. Blumenfeld, *Phys. Rev. E* **98**, 042905 (2018).
- [37] S. Ardanza-Trevijano, I. Zuriguel, R. Arevalo, and D. Maza, *Phys. Rev. E* **89**, 052212 (2014).